

Vision Based Docking of Multiple Satellites with an Uncooperative Target ^{*}

Fragiskos Furlas, Vignesh Kottayam Viswanathan,
Sumeet Satpute, and George Nikolakopoulos

*Robotics and AI Team
Luleå University of Technology, Luleå Sweden
E-mail: {frafou; vigkot; sumsat; geonik }@ltu.se*

Abstract: With the ever growing number of space debris in orbit, the need to prevent further space population is becoming more and more apparent. Refueling, servicing, inspection and deorbiting of spacecraft are some example missions that require precise navigation and docking in space. Having multiple, collaborating robots handling these tasks can greatly increase the efficiency of the mission in terms of time and cost. This article will introduce a modern and efficient control architecture for satellites on collaborative docking missions. The proposed architecture uses a centralized scheme that combines state-of-the-art, ad-hoc implementations of algorithms and techniques to maximize robustness and flexibility. It is based on a Model Predictive Controller (MPC) for which efficient cost function and constraint sets are designed to ensure a safe and accurate docking. A simulation environment is also presented to validate and test the proposed control scheme.

Keywords: Nonlinear cooperative control, Nonlinear model predictive control, Spacecraft docking, Visual navigation.

1. INTRODUCTION

1.1 Motivation

The subject of autonomous rendezvous and docking in space has become popular during the last decades. Successful proximity operations can be utilized to extend the life span of satellites and help with deorbiting when they reach end of life (EOL). The need of accurate pose estimation of uncooperative targets in space for navigation and docking is highlighted by the European Space Agency (ESA) hosting their Pose Estimation Challenge in 2019 (Kisantal et al., 2020). This challenge also enforced the use of only a single camera, highlighting the importance of simple, compact and cheap sensors for this kind of applications. Most of the published research on this topic focus on single-agent docking missions. With the recent advancements on the launch of small platforms and cansats, the use of multiple, smaller and simpler satellites can greatly increase the efficiency of the mission in terms of time and cost, which is the main motivation of the present article.

1.2 Related Works

A family of solutions for the ESA challenge used Convolutional Neural Networks (CNN) to estimate the pose of the target. However, the most popular implementations either require an a priori knowledge of the targets wireframe e.g. (Chen et al., 2019). Some solutions have also been

presented that lift this limitation e.g. (Proença and Gao, 2019). Nevertheless, the use of CNNs for pose estimation is still a relatively new field and require huge amounts of data for training.

More conventional solutions for the problem have been proposed in the literature. Zhao et al. (2021) splits these solutions into two categories: image-based and position-based. An example of an image-based solution, a controller built directly on the image taken by the sensor, is proposed by Huang et al. (2017). This work focuses on detecting well defined edges on spacecraft parts, such as brackets, where a mechanical grabber can easily attach. Martínez et al. (2017) propose matching a 3D model of the target with the output of on-board sensors but this method requires more complex LiDAR sensors. An effective and accurate way to estimate the pose of the target is to use markers on its surface. Christian et al. (2012) evaluated the use of special, reflective markers for docking purposes but still use complex combinations of LiDAR and camera sensors.

An example of a position-based approach is proposed by Volpe and Circi (2019) and is one of the most promising solutions in literature. It uses a combination of a pose estimation method based on the Structure from Motion (SfM) algorithm and an optimal control scheme, removing the need for markers and using only a monocular camera. But still, this work focuses on a single-agent docking scenario. Examples of docking multiple satellites exist in the literature but mostly focus on them docking with each other and not with an uncooperative target e.g. (Wang et al., 2003) and (Nunes et al., 2015).

^{*} © 2023 Fragiskos Furlas, Vignesh Kottayam Viswanathan, Sumeet Satpute, and George Nikolakopoulos. This work has been accepted to IFAC for publication under a Creative Commons Licence CC-BY-NC-ND

1.3 Contributions

The proposed framework in this work aims to integrate and present improvements based on aforementioned state-of-art works. Thus, the main contributions in this work are as follows:

- (1) We propose a novel centralized Nonlinear Model Predictive Controller architecture for multiple chaser spacecraft towards collaborative tracking and docking with an uncooperative, tumbling target spacecraft.
- (2) A robust, fault-tolerant, vision-based pose estimation framework
- (3) A comprehensive evaluations of the framework in a realistic simulation environment is carried out to prove the efficacy of the proposed work.

2. PROBLEM FORMULATION

The target is defined as an uncooperative object tumbling freely in 6-DOF, with constant velocities and with very simple markers imprinted on its body. The environment is considered as a frictionless, gravity-free, non-interacting, infinite space with sufficient lighting. A chaser is assumed to be a robotic system, capable of 6-DOF motion in the environment and equipped with a monocular camera. The odometry of the chaser is assumed to be known at any given time in relation to a static world frame.

The problem scenario discussed in this article is divided in to two parts. Initially, the synchronization problem is considered where the satellites will track the target and try to match it's tumbling path by maintaining a predefined pose *ref*, relative to the target. Later, satellites will slowly approach the target while maintaining their relative orientation until they are close enough to be considered docked to the target.

2.1 Reference Frames

The reference frames used are presented in Fig. (1).

WRF the *world frame*, is an arbitrary reference frame which will be used as a global reference.

CRF the *chaser frame* is a frame aligned with the chaser's chassis and fixed on its center of mass. The **X**-axis of *CRF* aligns with the direction that the chaser's camera is looking towards. The **Z**-axis points towards the top of the chaser's chassis and **Y**-axis completes the right handed coordinate frame.

TRF the *target frame* is a frame fixed at the center of mass of the target and arbitrarily aligned.

IRM the *image frame*, is a necessary transformation to properly align the reference frames with the notation used by OpenCV

2.2 System Dynamics

It is assumed that both the target and chasers are rigid bodies. In terms of inertial properties, target and chasers are considered to be rectangular cuboids as well as there are no gravity or any external forces are acting on the system.

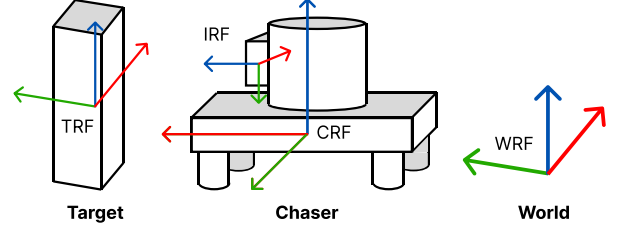


Fig. 1. The reference frames used in this work.

Chaser The chaser can be described as a rigid body with forces and/or torques acting on it's center of gravity representing thruster actuation. The chaser's state is defined by 13 variables: $p = [p_x, p_y, p_z]^T$ is the position, $q = [q_w, q_x, q_y, q_z]^T \in [-1, 1]^4$ is a rotation quaternion representing the orientation and $v = [\dot{p}_x, \dot{p}_y, \dot{p}_z]^T$ and $\omega = [\omega_x, \omega_y, \omega_z]^T$ are the linear and angular velocities in Euler form, respectively.

It is assumed that all the forces and torques are acting on its center of gravity and are relative to the *CRF* reference system. To model the physics of the chaser the Euler-Newton equations for translational and rotational dynamics of a rigid body (1) are used.

$$\begin{bmatrix} F \\ \tau \end{bmatrix} = \begin{bmatrix} mI_3 & 0 \\ 0 & I_{cm} \end{bmatrix} \begin{bmatrix} \dot{v}(t) \\ \dot{\omega}(t) \end{bmatrix} + \begin{bmatrix} 0 \\ \omega(t) \times (I_{cm} \cdot \omega(t)) \end{bmatrix} \quad (1)$$

where F and τ are the forces and torques acting on the bodys center of gravity, m and I_{cm} are the mass and the moment of inertia matrix of the body.

Equation. (2) presents the complete linear and angular dynamics of the chaser spacecraft.

$$\begin{cases} \dot{p}(t) = v(t) \\ \dot{v}(t) = \frac{1}{m} I_3 \hat{F} \\ \dot{q}(t) = -\frac{1}{2} \begin{bmatrix} 0 \\ \omega(t) \end{bmatrix} \otimes q(t) \\ \dot{\omega}(t) = I_{cm}^{-1} \cdot \hat{\tau} - I_{cm}^{-1} [\omega(t) \times (I_{cm} \cdot \omega(t))] \end{cases} \quad (2)$$

$\hat{\tau}$ and \hat{F} represent the forces and torques acting on the center of mass of the chaser rotated back to the *WRF* reference system. This can be performed by using the following equations (3) of quaternions rotating vectors:

$$\begin{aligned} \hat{F} &= qFq^* \\ \hat{\tau} &= q\tau q^* \end{aligned} \quad (3)$$

Target The target is also a rigid-body but with constant-velocity and no forces acting on it. The target has similar state variables to the chaser's, i.e. $[p^{tar}, q^{tar}, v^{tar}, \omega^{tar}]^T$ while the system dynamics can be described by (4).

$$\begin{cases} \dot{p}^{tar}(t) = v^{tar}(t) \\ \dot{v}^{tar}(t) = 0 \\ \dot{q}^{tar}(t) = -\frac{1}{2} \begin{bmatrix} 0 \\ \omega^{tar}(t) \end{bmatrix} \otimes q^{tar}(t) \\ \dot{\omega}^{tar}(t) = 0 \end{cases} \quad (4)$$

3. PROPOSED METHODOLOGY

To tackle the scenario at hand, a centralized control scheme was designed as shown in Fig. (2). Each chaser will process the images taken with its camera sensor on-board.

The images are un-distorted using a camera calibration model and then passed to the pose estimator.

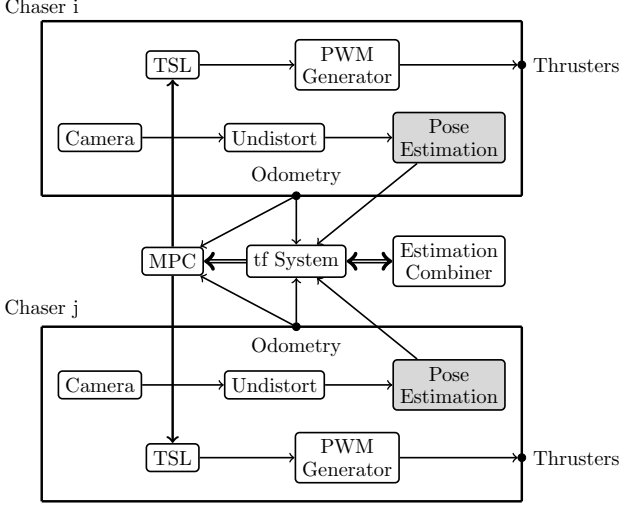


Fig. 2. Processing flow of a chaser swarm composed of two agents.

The pose estimator starts by detecting the ArUco markers (Garrido-Jurado et al., 2014), (Romero-Ramirez et al., 2018) imprinted on the target. The positions of the marker's corners in the TRF frame define a set P_{TRF} . The method for ArUco marker recognition allows extraction of the pixel coordinates of each individual corner of each marker. Each marker is also uniquely identifiable. A set P_{IRF} is defined containing these 2D coordinates of the corners visible on a given image capture.

Next, a Perspective-n-Point (PnP) problem is defined using P_{TRF} and P_{IRF} . The PnP problem is the problem of determining the pose of a calibrated camera given a set of n 3D points in the world and their corresponding 2D projections in the image (Kragic and Daniilidis, 2016; Wu and hu, 2006). Basically, solving the pinhole camera model in (5) for the extrinsic parameters ($[R|t]$), provided some 3D world coordinates (M) and 2D image coordinates (m) and with the intrinsic parameters (A) known.

$$sm' = A[R|t]M' \quad (5a)$$

$$s \begin{bmatrix} u \\ v \\ 1 \end{bmatrix} = \begin{bmatrix} f_x & 0 & c_x \\ 0 & f_y & c_y \\ 0 & 0 & 1 \end{bmatrix} \begin{bmatrix} R_{11} & R_{12} & R_{13} & T_1 \\ R_{21} & R_{22} & R_{23} & T_2 \\ R_{31} & R_{32} & R_{33} & T_3 \end{bmatrix} \begin{bmatrix} X \\ Y \\ Z \\ 1 \end{bmatrix} \quad (5b)$$

Implementations for both ArUco marker detection algorithm and the EPnP (Lepetit et al., 2008) solver used in this project were provided in the OpenCV library.

The target's pose estimations are sent to a TF system responsible for calculating transfer functions between different reference frames. An estimation combiner node is responsible to process the pose estimates of the chasers and to combine them into a single estimate for the targets odometry (pose & velocities). The combiner works by averaging the latest available estimations by each chaser that has line-of-sight to the target. It also uses a moving average filter for noise reduction, outlier detection and removal methods.

This combined estimation is fed, together with the chaser's odometry, to the controller. The controller then uses the estimated odometry to generate an optimal control signal for each chaser (see Ch. 4). The control signals, consisting of a set of 3-dimensional forces and torques, are sent to the chaser's Thruster Selection Logic (TSL) and finally to a Pulse Width Modulation (PWM) signal generator. The TSL module is considered as a black box for now and will be implemented later ad-hoc.

4. CONTROLLER

As previously mentioned, the control architecture uses a MPC backbone. In this section, the cost function and constraints used to formulate the MPC will be presented.

4.1 Cost Function

The chasers state vectors are defined as $x^i = [p^i, q^i]^\top$ and the corresponding control action as $u^i = [F^i, \tau^i]^\top$. The system dynamics are discretized with a sampling time of dt using the forward Euler method to obtain $x_{k+1}^i = \zeta(x_k^i, u_k^i)$. The target's state vector is defined as $x^{tar} = [p^{tar}, q^{tar}]$, where p^{tar} is the position and q^{tar} the quaternion attitude representation of the target. They are discretized in a manner similar to the chaser's states. The reference poses for the chasers are calculated by transferring the target's body frame using $x^{off_i} = [p^{off_i}, q^{off_i}]$, where p^{off_i} is a translation and q^{off_i} is a rotation quaternion. These calculations are performed as such: $p_k^{ref_i} = p_k^{tar} + q_k^{tar} \otimes p^{off_i} \otimes q_k^{tar*}$ and $q_k^{ref_i} = q_k^{tar} q^{off_i}$. This discrete model is used as the prediction model of the NMPC. The prediction is performed over a receding horizon of $D = T/dt$ steps, where T is the horizon duration in seconds.

A cost function is defined such that, when minimized in the current time and the predicted horizon, an optimal set of control actions u_k^i will be calculated. Let $x_{k+j|k}$ and $x_{k+j|k}^{tar}$ be the predicted chaser and target states at time step $k+j$ respectively, calculated in time step k . The corresponding control actions are $u_{k+j|k}$ and reference states $x_{k+j|k}^{ref_i}$. Also, let \mathbf{x}_k and \mathbf{u}_k be the predicted states and control actions for the whole horizon duration calculated at time step k . The cost function is formulated as follows:

$$J(\mathbf{x}_k, \mathbf{u}_k, u_{k-1|k}) = \sum_{i=0}^{N-1} \left\{ \sum_{j=0}^D \left\{ \underbrace{\left(1 - \frac{\alpha \cdot k}{D}\right)}_{\text{Falloff \%}} \cdot \left[\underbrace{\|p_{k+j|k}^{ref_i} - p_{k+j|k}^i\|^2}_{\text{Position cost}} Q_p + \underbrace{\|q_{k+j|k}^i \otimes q_{k+j|k}^{ref_i*}\|^2}_{\text{Orientation cost}} Q_q \right] \right. \right. \\ \left. \left. + \underbrace{\|u_{ref}^i - u_{k+j|k}^i\|^2}_{\text{Input cost}} Q_u \right\} \right. \\ \left. + \underbrace{\|p_{k+D|k}^{ref_i} - p_{k+D|k}^i\|^2}_{\text{Final state cost}} Q_p^f + \underbrace{\|q_{k+D|k}^i \otimes q_{k+D|k}^{ref_i*}\|^2}_{\text{Final state cost}} Q_q^f \right\} \quad (6)$$

where $Q_p, Q_p^f \in \mathbb{R}^{3 \times 3}$, $Q_q, Q_q^f \in \mathbb{R}^{4 \times 4}$ and $Q_u \in \mathbb{R}^{6 \times 6}$ are positive definite weight matrices for the position and

orientation states and inputs respectively. In (6), the first term represents the state cost which penalizes deviation from the reference state at time-step k , x_k^{ref} . The Falloff term α , is an adaptive weight to penalize overshoot errors. The second term represents the input cost which penalizes deviation from the steady-state input $u_{ref} = 0$ that describes constant-velocity movement. Finally, the final state-cost applies an extra penalty for deviation of the state from the reference at the end of the horizon period.

4.2 Constraints

A minimum chaser-chaser and chaser-target distance d_{min} is enforced by (7b) and (7c). (7d) prevents the chasers from moving too far away from the target by setting their maximum distance to d_{max} . The implemented constraints are the following:

$$u_{k+j|k}^i = [F_{k+j|k}^i, \tau_{k+j|k}^i] \in [-F_{max}, F_{max}] \times [-\tau_{max}, \tau_{max}] \quad (7a)$$

$$\text{dist}(p_{k+j|k}^{tar}, p_{k+j|k}^m) \geq d_{min} \quad \forall j \in [0, D] \quad (7b)$$

$$\text{dist}(p_{k+j|k}^m, p_{k+j|k}^n) \geq d_{min} \quad \forall j \in [0, D], m \neq n \quad (7c)$$

$$\text{dist}(p_{k+j|k}^{ref}, p_{k+j|k}^m) \leq d_{max} \quad \forall j \in [0, D] \quad (7d)$$

where dist is a function of Euclidean distance.

4.3 Optimizer

Optimization Engine (OpEn) was used as the MPC cost function optimizer. OpEn is a framework developed by Sopaşakis et al. (2020) and is based on the PANOC (Stella et al., 2017) optimization algorithm. PANOC is an extremely fast, the state-of-the-art optimizer for real-time, embedded applications. A powerful symbolic mathematics library called CasADi (Andersson et al., In Press, 2018) is used to define the optimization problem and perform under-the-hood operations.

5. SIMULATION RESULTS

The following section presents the results of the simulations that were performed to test the control architecture. First of all, in Section 5.1 different parameters of the MPC controller are tested and compared in a single chaser scenario. Then, in Section 5.2 multi chaser scenarios are performed and the docking sequence is tested. Finally, in Section 5.3 a clear demonstration of the collision avoidance capabilities are presented. In every scenario the velocities of the target are $v = [1.50, 0.75, 3.00] \times 10^{-2} \text{m/s}$ and $\omega = [1.50, 4.50, 3.00] \times 10^{-2} \text{rad/s}$ and the simulations were recorded over 2 minutes. A video demonstration of these simulations can be found at youtu.be/86JT4M7eyGc.

5.1 Single Chaser & MPC Tuning

The tuneable parameters of a MPC controller are the cost function parameters described in (6). The error terms of each state variable, scaled by their weight Q_p , need to be close to each other to avoid some to be prioritized over

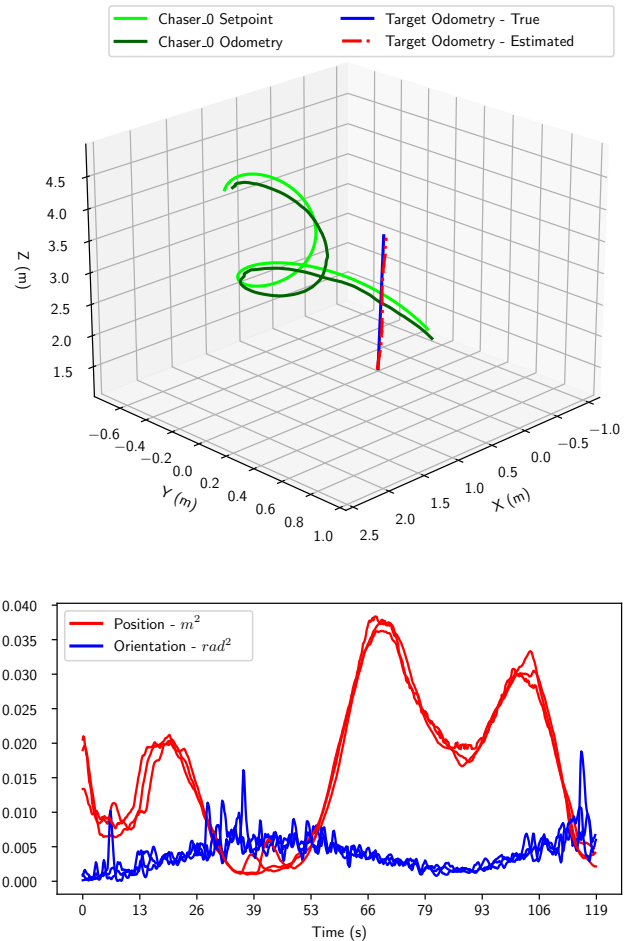


Fig. 3. Baseline runs with 1 chaser, $T = 3\text{s}$, $dt = 0.1\text{s}$ and $\alpha = 0\%$. **Top:** Chaser and target trajectories, **Bottom:** Pose errors.

others. For example in cases where the chasers start far away from the target, the position error will be degrees of magnitude higher than the quaternion error which is bounded in $[-1, 1]$. The Q_u weights penalize the use of the control inputs and can be tuned by trail and error to avoid over-actuation of the chaser. Finally the Q_f weights penalize the final state error to avoid overshooting the target and must be tuned higher than Q_p .

	Q_p	Q_u	Q_f
Position/Force	65	3.5	3250
Orientation/Torque	35	40	1750

Table 1. MPC Tuning Weights

The values of these weights are presented in Table 1 and were determined after repetitive testing. The rest of the cost function parameters have more interesting effects on the performance of the controller and thus are further analyzed in the following subsections. As a baseline for comparison, Figure 3 shows the results of the MPC controller with $T = 3\text{s}$, $dt = 0.1\text{s}$ and $\alpha = 0\%$. Every test was performed and recorded three times for more accurate results. Table 2 presents the results of the simulations.

² Average over 3 runs.

³ 1/3 runs failed.

⁴ 2/3 runs failed.

<i>Comment</i>	<i>T</i> (s)	<i>dt</i> (s)	α (%)	Position ¹ <i>MSE</i>	Orientation <i>MSE</i>
Baseline	3	1/10	0%	1.64	3.94
<i>T</i> test	0.5	1/10	0%	64.8 ²	229
	10	1/10	0%	126 ³	943
<i>dt</i> test	3	1/5	0%	1.73	4.87
	3	1/30	0%	1.42	3.89
α test	3	1/10	10%	1.65	4.09
	3	1/10	30%	1.69	4.07
	3	1/10	60%	1.75	4.25
	3	1/30	30%	1.59	4.02

Table 2. Single Chaser Tests. Position MSE: $m^2 \times 10^{-2}$, Orientation MSE: $rad^2 \times 10^{-3}$

Horizon Period: T is the time in seconds that the controller will predict the future of the system. It is clear that T is the most important parameter for tuning the MPC controller. Having too small a horizon allows the controller to predict only the short term results of the plant's input and too large a horizon will make the controller too slow. Both tests with $T = 0.5s$ and $T = 10s$ had failed runs.

Prediction Time Step: dt is the sampling for the horizon period. Smaller dt values will make the controller more accurate since it improves the performance of the forward Euler method. Decreasing dt also adds more steps to the MPC and thus more variables in the optimization problem, increasing the calculation time for a solution.

Falloff percentage: The experimental term α is tested for performance improvement. The test results show that α actually increases the MSE of every scenario and thus is not used in the final controller.

5.2 Multi Chaser

For multi chaser scenarios, two tests were performed. The first test is a simple tracking scenario where two chasers communicate their estimations of the target's pose to each other to maintain a pre-defined pose relative to the target. In Figure 4, a spike in the MSE plot is observed at around 100s, which is caused by a Euler angle singularity introduced by the PnP solver of OpenCV. This singularity can be interpreted as a random interference in the system which the controller was able to handle, hence showcasing it's robustness.

The second test is a more complex scenario where four chasers initially track the target. After about 60s Chaser 0 and 3 receive an approach command and start docking the target. Their relative pose is maintained throughout the docking process but their position is gradually scaled to decrease their distance to the target. Figure 5 showcases the distance each chaser maintains from the target. Of course the pose error increases in the docking process since the chaser's position is compared to their initial ref pose and not the docking pose.

5.3 Collision Avoidance

To showcase the collision avoidance capabilities of the controller, a simple scenario was created where two chasers are initially just tracking a stationary target. A command

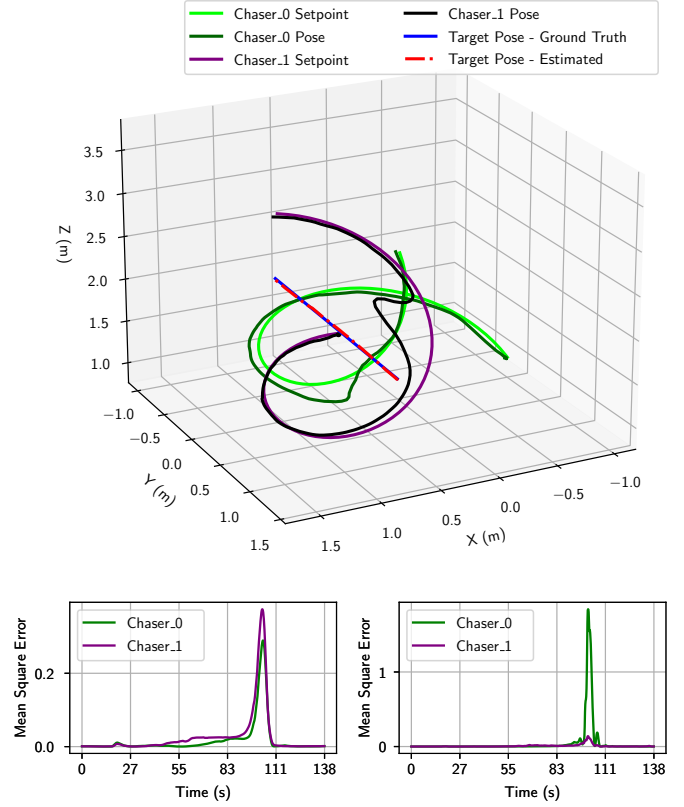


Fig. 4. Two Chaser tracking mission. **Top:** Chaser and target trajectories, **Bottom left:** Chaser position error, **Bottom right:** Chaser orientation error

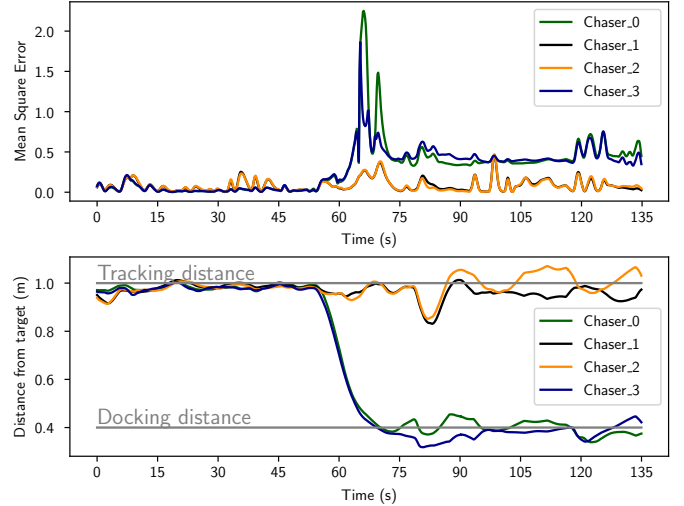


Fig. 5. Four Chaser tracking mission with Chaser 0 and 3 docking after 60 seconds. **Top:** Chasers pose error, **Bottom:** Docking evaluation

is given to Chaser 0 to change it's ref pose to a position on the opposite side of the target. The closest route to that pose would be a direct line through the target. However, the controller is able to find a path over the target, respecting a limit of $d_{min} = 0.35m$. Chaser 1 maintains it's initial ref pose relative to the static target, observing the scene from afar. This is crucial since Chaser 0 will inevitably loose sight of the target and be unable to

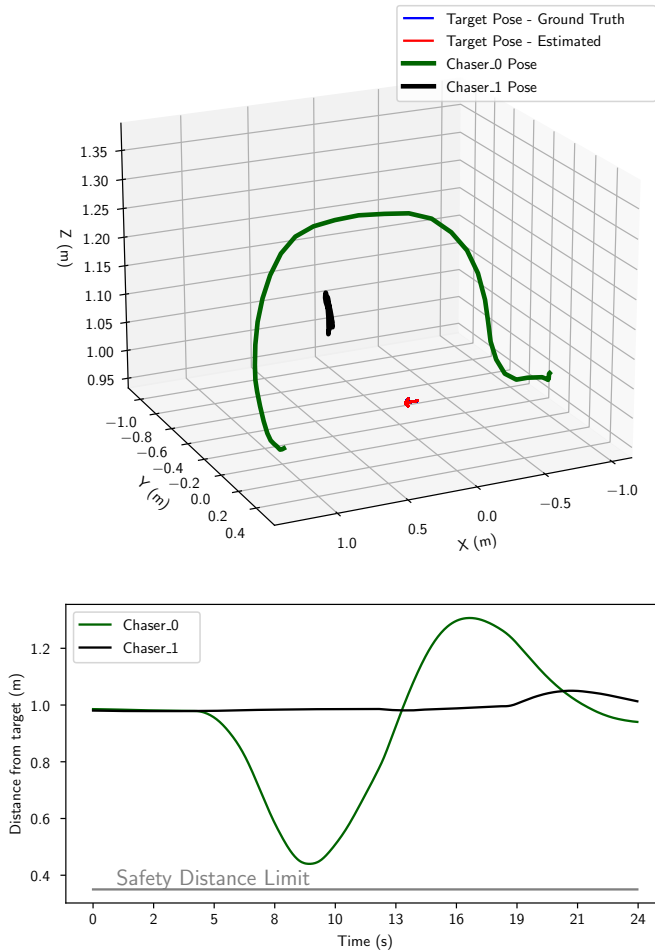


Fig. 6. Two Chaser, collision avoidance mission. Chaser 0 maneuvers over the target while Chaser 1 assists with visual pose estimation. **Top:** Chaser trajectories and Target pose, **Bottom:** Collision avoidance evaluation

estimate it's pose alone. The pose estimation from Chaser 1 is used by Chaser 0 during the maneuver, showcasing one of the benefits of the multi chaser approach.

6. CONCLUSION

In this article we propose a reliable centralized NMPC-based control architecture that can assist in docking of multiple chaser spacecraft to a tumbling target in Space. The tumbling target pose is estimated using a single monocular camera on-board each chaser spacecraft. The estimated pose is shared between the chaser spacecraft to improve the fused pose estimate of the target when the target moves of the field of view of one of the chaser spacecraft. Multiple simulation scenarios were tested to determine the efficacy of the proposed controller.

REFERENCES

Andersson, J.A.E., Gillis, J., Horn, G., Rawlings, J.B., and Diehl, M. (In Press, 2018). CasADi – A software framework for nonlinear optimization and optimal control. *Mathematical Programming Computation*.

Chen, B., Cao, J., Bustos, Á.P., and Chin, T. (2019). Satellite pose estimation with deep landmark regression and nonlinear pose refinement. *CoRR*, abs/1908.11542.

Christian, J., Patangan, M., Hinkel, H., Chevray, K., and Brazzel, J. (2012). *Comparison of Orion Vision Navigation Sensor Performance from STS-134 and the Space Operations Simulation Center*.

Garrido-Jurado, S., Muñoz-Salinas, R., Madrid-Cuevas, F., and Marín-Jiménez, M. (2014). Automatic generation and detection of highly reliable fiducial markers under occlusion. *Pattern Recognition*, 47(6), 2280–2292.

Huang, P., Chen, L., Zhang, B., Meng, Z., and Liu, Z. (2017). Autonomous rendezvous and docking with non-full field of view for tethered space robot. *International Journal of Aerospace Engineering*, 2017, 3162349.

Kisantal, M., Sharma, S., Park, T.H., Izzo, D., Märten, M., and D'Amico, S. (2020). Satellite pose estimation challenge: Dataset, competition design, and results. *IEEE Transactions on Aerospace and Electronic Systems*, 56(5), 4083–4098.

Kragic, D. and Daniilidis, K. (2016). 3-d vision for navigation and grasping. In B. Siciliano and O. Khatib (eds.), *Springer Handbook of Robotics*, chapter 32, 811–824. Springer, Verlag Berlin Heidelberg.

Lepetit, V., Moreno-Noguer, F., and Fua, P. (2008). Epnp: An accurate o(n) solution to the pnp problem. *International Journal of Computer Vision*, 81(155), 155–166.

Martínez, H.G., Giorgi, G., and Eissfeller, B. (2017). Pose estimation and tracking of non-cooperative rocket bodies using time-of-flight cameras. *Acta Astronautica*, 139, 165–175.

Nunes, M.A., Sorensen, T.C., and Pilger, E.J. (2015). *On the development of a 6DoF GNC framework for docking multiple small satellites*.

Proença, P.F. and Gao, Y. (2019). Deep learning for spacecraft pose estimation from photorealistic rendering. *CoRR*, abs/1907.04298.

Romero-Ramirez, F.J., Muñoz-Salinas, R., and Medina-Carnicer, R. (2018). Speeded up detection of squared fiducial markers. *Image and Vision Computing*, 76, 38–47.

Sopasakis, P., Fresk, E., and Patrinos, P. (2020). OpEn: Code generation for embedded nonconvex optimization. In *IFAC World Congress*. Berlin.

Stella, L., Themelis, A., Sopasakis, P., and Patrinos, P. (2017). A simple and efficient algorithm for nonlinear model predictive control.

Volpe, R. and Cenci, C. (2019). Optical-aided, autonomous and optimal space rendezvous with a non-cooperative target. *Acta Astronautica*, 157, 528–540.

Wang, P., Mokuno, M., and Hadaegh, F. (2003). *Formation Flying of Multiple Spacecraft with Automatic Rendezvous and Docking Capability*.

Wu, Y. and hu, Z. (2006). Pnp problem revisited. *Journal of Mathematical Imaging and Vision*, 24, 131–141.

Zhao, X., Emami, M.R., and Zhang, S. (2021). Image-based control for rendezvous and synchronization with a tumbling space debris. *Acta Astronautica*, 179, 56–68.